Hindawi Publishing Corporation
Journal of Nanomaterials
Volume 2014, Article ID 962102, 12 pages
http://dx.doi.org/10.1155/2014/962102

Research Article

Comparison between Base Metals and Platinum Group Metals in Nitrogen, M Codoped TiO_2 (M = Fe, Cu, Pd, Os) for Photocatalytic Removal of an Organic Dye in Water

Alex T. Kuvarega,[1] Rui W. M. Krause,[2] and Bhekie B. Mamba[1]

[1] *Nanotechnology and Water Sustainability Research Unit, College of Engineering, Science and Technology, University of South Africa, Florida Campus, Johannesburg 1709, South Africa*
[2] *Department of Chemistry, Rhodes University, P.O. Box 94, Grahamstown 6140, South Africa*

Correspondence should be addressed to Bhekie B. Mamba; mambabb@unisa.ac.za

Received 22 April 2014; Accepted 7 October 2014; Published 27 October 2014

Academic Editor: Takuya Tsuzuki

The photocatalytic performance of a number of nonmetal and metal codoped TiO_2 for the degradation of eosin yellow under simulated solar radiation was investigated. The synthesised materials were characterised by FTIR, Raman spectroscopy, XRD, DRUV-Vis, SEM, and TEM. The N, metal codoped TiO_2 containing 0.5 wt.% of the metal consisted mainly of the anatase phase, with a particle size range of 15–28 nm. The particles were largely spherical and shifted the absorption edge well into the visible region. Band gap reduction was more pronounced for the N, PGM codoped TiO_2 compared to N, base metal codoped samples. Codoping led to an enhancement in the photocatalytic activity of the materials for the degradation of eosin yellow. N, Pd codoped TiO_2 was the most effective photocatalyst (99.9% dye removal) while N, Cu codoped TiO_2 showed the least activity (25.5% removal). The mechanism for the photocatalytic enhancement was proposed on the basis of formation of an electron deficient Schottky barrier at the semiconductor-metal interface, which acts as an electron sink and thus retards electron-hole recombination. It was shown that the ability of the photocatalyst to degrade the dye depends on the nature and type of the metal dopant in the codoped TiO_2 system.

1. Introduction

Any large-scale scheme to harvest solar energy for sustainable environmental clean-up will most likely include the use of TiO_2, an extensively studied potential candidate for a wide range of environmental applications, including water decontamination. Use of pure TiO_2 is hampered by its wide band gap (3.2 eV) which has limited its photocatalytic use in real life water treatment systems [1, 2]. To address these challenges, much effort is being devoted to the manipulation and modification of the TiO_2 lattice structure with a view of utilising the abundant natural sunlight for decontaminating polluted water [3]. The effective utilisation of clean, cheap, safe, and abundant solar energy promises to be an excellent option for tackling global challenges related to environmental pollution remediation and sustainability [4]. In general, researchers are concentrating on two aspects of TiO_2 related to its performance: enhancing the photocatalytic efficiency and extending the absorption edge to the visible region [2, 5, 6].

Various methods have been reported on improvement of the photoactivity of TiO_2. Among them, doping with transition metals has proved to be favourable though the metals, in some cases, were found to act as recombination centres resulting in reduced photoactivity [2]. The photocatalytic reactivity of TiO_2 is remarkably enhanced by doping small amounts of base metals such as Fe, Cu, V, Mo, or Ni and noble metals such as Pt, Pd, Os, Ir, Ru, or Rh. Doping with metals is believed to result in an overlap of the Ti 3d orbitals with the d levels of the metals causing a bathochromic effect in the absorption band edge of TiO_2. This band gap shift favours the use of visible light to activate the TiO_2 depending on the type of metal dopant and its concentration. The Fermi levels of these metals are also lower than those

of TiO_2; therefore, photoexcited electrons can be transferred from conduction band to metal particles deposited on the surface of TiO_2. The overall effect is reduction of electron-hole recombination, resulting in efficient charge separation and higher photocatalytic activities [2, 4]. Optimal loading of metal must be taken into consideration since high levels of metal particle deposition might reduce photon absorption by TiO_2 or the metal centres become electron-hole recombination sites, negatively affecting efficiency [7, 8]. Since noble metals are scarce and very expensive, more research is needed to find low cost metals with improved photocatalytic activity. Base metals such as Fe and Cu have been shown to trap not only electrons but also holes when the impurity energy levels introduced are near conduction band as well as the valence band edge of TiO_2 [4]. For that reason, doping of either Fe or Cu ions is recommended as these low cost metals may show similar or even better enhancement of photocatalytic activity compared to the rather expensive noble metals that can only trap one type of charge carrier. These base metals may become promising alternative TiO_2 dopants for enhanced photocatalytic water decontamination applications. Metal ion dopants such as Fe^{3+} and Os^{4+} can possibly substitute some Ti^{4+} sites within TiO_2 lattice because their ionic radii (0.64 Å for Fe^{3+} and 0.63 Å for Os^{4+}) are a bit smaller than those of Ti^{4+} (0.68 Å). Such metals are also favourable candidates for doping as they can easily attain half-filled electronic configurtions in their most stable ionic states [9]. In contrast, Cu^{2+} and Pd^{2+} will most likely be located on interstitial positions of the lattice rather than directly on Ti^{4+} sites because of their relatively larger ionic sizes (0.72 Å for Cu^{2+} Å and 0.86 Å Pd^{2+}) compared to Ti^{4+} [10, 11].

The use of anion doping to improve photocatalytic activity of TiO_2 under visible light is increasing. One of the most promising and widely investigated materials for visible photocatalysis is nitrogen doped TiO_2 although other anions such as F, B, C, P, and S have also been found to enhance the photocatalytic activity of TiO_2 in the visible range. Unlike metals, anions form less likely recombination centres and are therefore more effective in enhancing the photoactivity [6, 12–14]. However, the mechanism behind the photocatalytic enhancement still remains nebulous. Motivated by the positive photocatalytic response realised through nonmetal and metal doping of TiO_2, strategies aimed at further enhancing the quantum efficiency of the TiO_2-based materials saw the sprouting of a material engineering technique known as codoping. This TiO_2 modification technique has gained wide attention in recent years [11, 15–19]. Taking advantage of the possible synergistic effects on the photocatalytic activity of the material, various forms of double metal dopants, double nonmetal dopants, double metal, nonmetal dopants, and even tridopants have been introduced on TiO_2 [20–23]. The objective in many of these studies is to advance the material engineering of TiO_2 by altering the optical properties through specially designing trap sites for both electrons and holes as well as reducing the band gap [24]. Besides shifting the absorption edge of TiO_2 successfully from the ultraviolet region to the visible light region, codoping also improves the physical properties of TiO_2 such as specific surface area and crystallite size whilst prohibiting the anatase to rutile phase transformation [25]. Liu and Gao [11] reported a S, N codoped TiO_2 photocatalyst which showed better photocatalytic activity than singly doped S and N TiO_2 for degradation of methylene blue solution under visible light. Sakatani et al. [17] successfully synthesised N, Sr codoped TiO_2, for visible light photocatalytic degradation of acetaldehyde. They observed enhanced activity for the codoped sample among a group of studied metal ions. Such observations may open up new possibilities for the development of efficient solar induced photocatalytic materials. However, until now, there are only a few reports on anion, metal codoped TiO_2 [17, 18]. There is still need for fabrication of chemically stable and highly active photocatalyst that could work in the visible range.

Currently, there are a limited number of reports on comparative study of environmental applications of nonmetal, platinum group metal codoped TiO_2 with nonmetal, base metal codoped TiO_2. The nonmetal, metal codoping of TiO_2 is envisaged to result in a material with excellent photocatalytic performance compared to singly- or monodoped TiO_2. This study reports the sol-gel synthesis of (N, Pd) codoped TiO_2, (N, Os) codoped TiO_2, (N, Fe) codoped TiO_2, and (N, Cu) codoped TiO_2 nanomaterials and comparison of their photocatalytic activities for degradation of aqueous eosin yellow (EY) dye under simulated solar light. EY was selected because of its stability to photolysis by solar radiation. Its absorbance is also not affected by pH changes in the range 3–9.

2. Materials and Methods

2.1. Synthesis of N, Os Codoped TiO_2. A modified sol-gel method in which ammonium hydroxide was used as both a source of nitrogen and a hydrolysing reagent was adopted. Briefly, osmium tetroxide, OsO_4 (1 g) (Sigma, USA) was dissolved in 2-propanol (50 mL). An appropriate amount of this solution was added to a mixture of 2-propanol C_3H_8O, (50 mL) (99.8%, Sigma Aldrich, Germany) and titanium isopropoxide, $Ti(OC_3H_7)_4$ (10 mL) (97%, Sigma Aldrich, Germany) to give an Os : Ti percentage of 0.5% and then ammonia, NH_3 (3 mL of 25%) (Merck, Germany) was slowly added to the isopropoxide/2-propanol solution with vigorous stirring for about half an hour and stirring continued until the solution became homogenous. The resulting sol was dried in air at 80°C for 12 hours and then calcined for 2 hours in air at 500°C in an electric furnace. The sample was then characterised by various methods.

2.2. Synthesis of N, Pd Codoped TiO_2, N, Fe Codoped TiO_2, and N, Cu Codoped TiO_2. A similar procedure was followed for the other codoped samples with slight variations in the nature of the metal precursor as well as the sequence of solution addition. For N, Pd TiO_2, an appropriate amount of palladium diammine dichloride, $Pd(NH_3)_2Cl_2$ (45% Pd, PGM Chemicals, RSA) to give a Pd : Ti proportion of 0.5%, was dissolved in 3 mL of 25% ammonia, NH_3 (Merck, Germany), prior to addition to the isopropoxide/2-propanol mixture while, for N, Fe TiO_2 and N, Cu TiO_2, appropriate

amounts of $Fe(NO_3)_2{\cdot}9H_2O$ (>98%, Sigma Aldrich, Germany) and $Cu(NO_3)_2{\cdot}6H_2O$ (99.5%, Merck, Germany) to give the metal : Ti proportion of 0.5% were dissolved in the 2-propanol (50 mL) used as a solvent for the isopropoxide prior to addition of the 3 mL of 25% ammonia. Samples were then treated the same way as for the N, Os codoped TiO_2. The N doped TiO_2 sample was prepared by following the same procedure without the addition of any metal precursors.

2.3. Characterisation. The morphology of the materials was characterized by imaging on a field emission scanning electron microscope (NOVA FEI/FIB FE-SEM) equipped with an INCA EDS for elemental analysis and on a transmission electron microscope (Tecnai G^2 Spirit TEM). Raman spectra were acquired on a Czerny-Turner micro-Raman spectrometer (Perkin Elmer Raman microscope) with excitation laser beam of wavelength 785 nm equipped with a cooled charged coupled device (CCD) detector set at −50°C and an Olympus BX51M microscope. The beam path was set to 50X and exposure time to 5 seconds during data acquisition. X-ray diffraction (XRD) experiments were conducted to identify the crystalline phases and estimate particle sizes of the codoped samples using a Philips PANalytical X'pert X-ray diffractometer, operated at 40 kV and 40 mA. Nickel filtered Cu K_α radiation (λ = 0.15406 nm) was used as the source. Particle sizes were estimated by applying the Scherrer equation using the full width at half maximum of the most intense peak. Fourier transform infrared spectroscopy (FTIR) was used to verify the bond vibrations related to functionalities on the materials. A Perkin Elmer, Spectrum 100, was used and samples were thinly mounted in their powder form on a NaCl window sample accessory and a number of spectra averaged at a resolution of 4 cm^{-1}. Diffuse reflectance data were obtained on a Shimadzu UV 2450 spectrophotometer equipped with an IRS 240 integrating sphere. $BaSO_4$ was used as the reflectance standard. Reflectance data were used to plot Kubelka-Munk and Tauc plots for band gap estimations.

2.4. Evaluation of Photocatalytic Activity. The photocatalytic activities of the materials were measured by the photodegradation of eosin yellow (EY) under simulated solar illumination using an AM 1.5 solar simulator (Oriel, Newport) set at an intensity of 1000 Wm^{-2} (1 sun). The solar simulator is equipped with an Oriel 500 W Xenon lamp as a source of radiation. A reference cell (Oriel PV system equipped with a 2 cm × 2 cm monocrystalline silicon photovoltaic cell and a Type K thermocouple) was used to set the simulator irradiance to 1 sun. A portion of the sample (0.1 g) was added to 100 mL of 100 ppm EY solution followed by sonication for about 10 minutes. The suspension was then stirred in the dark for an hour to allow for adsorption-desorption equilibrium before illumination. Aliquots (3 mL) were then sampled every 15 minutes and filtered through a 0.22 μm PVDF membrane filter for 180 minutes. Variations in EY concentration under illumination were then monitored using a Shimadzu UV-2450 spectrophotometer at the wavelength of maximum absorption of the dye (517 nm).

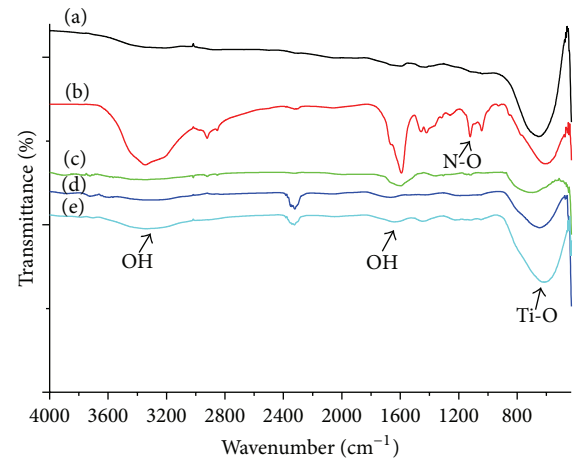

Figure 1: FTIR spectra of (a) P25, (b) N, Pd TiO_2, (c) N, Fe TiO_2, (d) N, Os TiO_2, and (e) N, Cu TiO_2.

3. Results and Discussion

Presence of functionalities on the materials was confirmed by FTIR (Figure 1). Peaks at 3340 cm^{-1} and 1636 cm^{-1} can be ascribed to OH stretching and the OH bending vibrations of absorbed water molecules and the surface hydroxyls on the TiO_2 particles, respectively. These surface hydroxyl groups play an important role in the photocatalytic process because they act as molecule adsorption centres as well as hole scavenging sites for the generation of hydroxyl radicals with high oxidation capability [26]. The N, Pd TiO_2 showed highly intense vibrations compared to the other samples. In addition, there were also peaks at 1120 cm^{-1} and 1030 cm^{-1} which can be ascribed to the N–O vibrations. Small peak at 2896 cm^{-1} can be assigned to CH_3 and CH_2 stretching vibration, implying that some organic moieties still existed in the sample. The broad peak in the range 750–520 cm^{-1}, observed in all the samples, is due to stretching vibration of Ti–O. The codoped samples exhibited wider peaks as compared to pure commercial P25 in the higher wavenumber region.

Raman spectroscopy is a powerful technique for investigating various phases of crystalline TiO_2 or its modified forms. The technique is capable of elucidating the photocatalyst structural complexity as phase peaks from each material are clearly separated in frequency and therefore easily distinguishable [27]. Four peaks were observed for all the codoped samples at wavenumbers 145, 395, 515, and 640 cm^{-1} and are attributed to the strong E_g, the medium strength B_{1g}, the A_{1g}, and an E_g Raman mode, respectively (Figure 2). These observations are consistent with reported fundamental Raman peaks of anatase TiO_2 [28]. In contrast, the rutile phase which consists of weak features at 142 cm^{-1}, 320 cm^{-1}, 357 cm^{-1}, and 826 cm^{-1} and stronger peaks at 447 cm^{-1} and 612 cm^{-1} could not be clearly detected, though some of the samples were shown, through XRD analysis, to be containing a small percentage of the rutile phase [29]. This can be attributed to the low percentage rutile phase in all the samples. Commercial TiO_2 (P25) consists of about

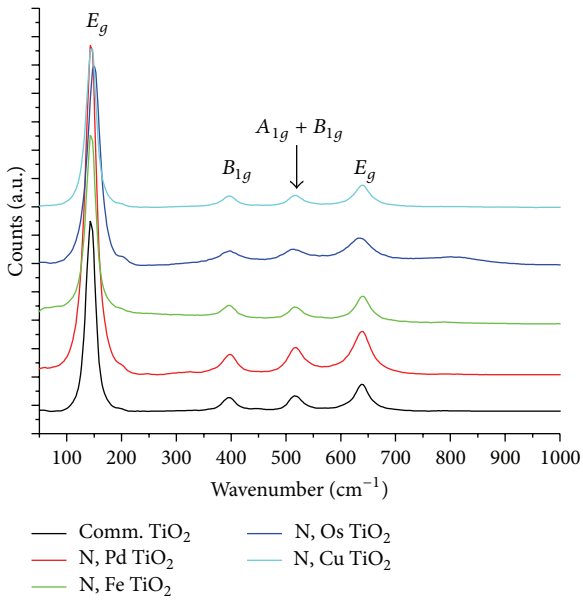

Figure 2: Raman spectra of the various samples.

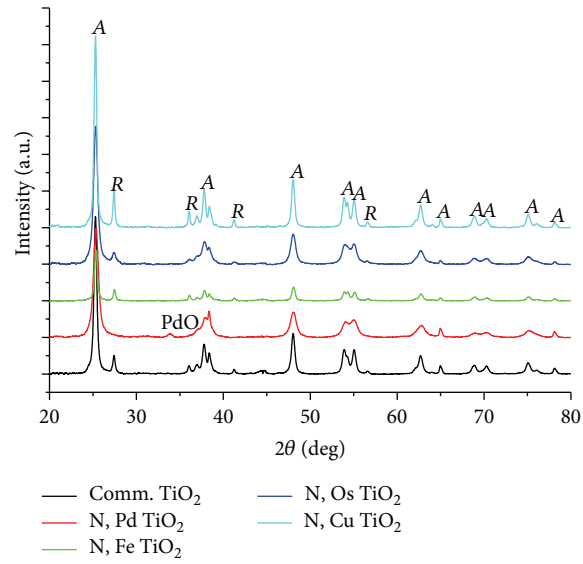

Figure 3: XRD spectra of the different codoped samples.

80% anatase and 20% rutile. The strong E_g band for N, Os TiO_2 is shifted to higher wavenumber value of about 150 cm^{-1}, evidence of substitutional doping of Os on the TiO_2 lattice. PdO has two known Raman active modes ascribed to the B_{1g} and the E_g. These modes are assigned to lines at 651 cm^{-1} (B_{1g}) and 445 cm^{-1} (E_g). The highly intense B_{1g} mode is due to scattering from the (001) face and the E_g mode from the (110) face. There is possibility of overlap between the highly intense anatase E_g line with the B_{1g} of PdO since they appear in the same wavenumber region. The PdO E_g line is less intense and could not be detected at low Pd loadings used in this study. However, XRD analysis (Figure 3) confirmed the presence of PdO in the N, Pd codoped sample. No Raman lines due to individual metals or their oxides were observed in the nitrogen, metal codoped samples. This may prove even dispersion of the metals on the TiO_2 lattice, with no segregations or clusters. This may also be due to the presence of the metal dopants in low concentrations on the crystal lattice [30].

The XRD patterns of crystalline materials are shown in Figure 3. The peaks at 2θ values of 25.3, 37.8, 48.0, 53.9, 55.1, 62.7, 68.8, 70.3, and 75.0° can be indexed to (101), (004), (200), (105), (211), (204), (116), (220), and (215) crystal planes of anatase TiO_2, respectively [29]. In addition, characteristic diffraction peaks at 27.4, 36.1, and 41.2° were also observed for the P25, N, Fe TiO_2, N, Os TiO_2, and N, Cu TiO_2 and are attributed to the (110), (101), and (111) faces of the rutile phases. The rutile peaks were more pronounced for the N, Cu TiO_2 indicating a higher percentage of that phase in this sample. The presence of Pd inhibited the anatase to rutile transformation as shown by the low rutile percentage (2.7%) in the N, Pd codoped sample. This is ascribed to the formation of defects at the grain boundaries of the TiO_2 resulting in distortion of ordering and consequently suppression of the anatase to rutile transformation. The dispersed PdO particles on the anatase phase (detected by XRD and TEM analyses) inhibited the rutile phase formation. The significant growth of PdO phase diminished rutile phase proportion in the sample and this reflects that codoping critically influences TiO_2 phase transformations [31]. All the other codoped samples showed an appreciable amount of the rutile phase (> 10%). Notably, no typical diffraction peaks for the nonmetal or metal dopants were observed in all the samples except a tiny peak at 2θ value of 33.8° attributed to the (101) plane of PdO for the N, Pd TiO_2.

The principal and most intense anatase peak (101) at 25.3° was used to determine the average crystallite size of the samples using the Scherrer equation:

$$d = \frac{k\lambda}{B\cos\theta}, \quad (1)$$

where d is the crystalline size, λ is the X-ray wavelength, B is the full width at half maximum of the peak, θ is the incident angle, and k is a shape factor [27, 32].

The phase composition of samples was calculated using the following formula:

$$X_A = \left[1 + \frac{I_R}{0.79\,(I_A)}\right]^{-1}, \quad (2)$$

where X_A is the percentage content of anatase, I_A is the intensity of the anatase (101) peak, and I_R is the intensity of the rutile (110) peak [33]. The calculated crystallite sizes and phase composition of the samples are shown in Table 1. The present PGMs inhibited crystal growth as shown by the small crystallite sizes. The PGM codoped samples showed smaller particle sizes compared to base metal codoped samples.

The effect of doping on the optical properties of the materials was evaluated by diffuse reflectance UV-Vis spectroscopy. The presence of different metal dopants significantly affected the light absorption pattern of the codoped

Table 1: Particle size and phase composition of the materials.

Sample	Particle size (nm)	Anatase phase (%)
Commercial TiO_2 (P25)	26.7	79.2
N, Pd codoped TiO_2	15.8	97.3
N, Fe codoped TiO_2	26.2	85.8
N, Os codoped TiO_2	14.0	87.9
N, Cu codoped TiO_2	24.9	72.1

Table 2: Optical band gaps of the materials.

Sample	Optical band gap (eV)
Comm. TiO_2 (P25)	3.1
N TiO_2	2.7
N, Pd TiO_2	2.1
N, Fe TiO_2	2.6
N, Os TiO_2	2.0
N, Cu TiO_2	2.8

samples (Figure 4(a)). All samples were characterised by an intense absorption in the UV region (300–400 nm). This fundamental absorption is associated with an electron transition from the valence band to the conduction band in TiO_2. Doping with nitrogen, base metals or PGMs led to red shifts in the absorption edge of the materials. The red shift appeared more pronounced for the N, PGM codoped samples compared to the N, base metal codoped samples and N doped sample. The red shift in the absorption edge is due to the formation of intraband gap impurity energy levels between the valence and the conduction band of TiO_2, narrowing the semiconductor band gap. The red shift in the absorption edge in the codoped TiO_2 can then be attributed to the charge-transfer transition between the nitrogen p or metal d electrons and the TiO_2 conduction or valence band. Metal doping has been reported to result in formation of dopant energy levels within the band gap of TiO_2. Electronic transitions from the valence band to the dopant level or from the dopant level to the conduction band of TiO_2 can lead to a red shift in the absorption band edge [27]. Doping with nitrogen increased the absorption intensity of N TiO_2 into the visible spectral region (>400 nm). The absorption centred at about 500 nm is mainly due to the N 2p to Ti 3d transition. N, Cu codoped TiO_2 showed an absorption band centred at 850 nm in addition to an increase of absorption at 400–550 nm compared to P25. These absorption bands are attributed to the d-d transitions of Cu. An increase of absorption at 350–500 nm with an absorption tail at 500–800 nm was observed in the case of N, Fe codoped TiO_2. Again, these are attributed to the d-d transition of Fe. Similarly, N, Pd, and N, Os codoped TiO_2 also exhibited increased visible range absorption which can be attributed to d-d transitions. There is possibility of these metals appearing as oxides on the N TiO_2, an observation supported by the existence of PdO peak in the XRD spectra of N, Pd codoped TiO_2 [34].

The reflectance data were converted to absorption coefficient and Kubelka-Munk plots generated from the data (Figure 4(b)). Presence of TiO_2 could be inferred from the absorption in the UV spectral region because of the large band gap of 3.2 eV for the anatase phase. Generally, the N, PGM codoped TiO_2 showed higher absorption in the lower UV region (200–250 nm) compared to the other samples with N, Pd codoped TiO_2 exhibiting the highest absorption while N, Cu codoped TiO_2 had the least UV absorption. Solar radiation is reported to consist of about 5% UV radiation, which is too low to be the main reason for enhanced photocatalytic activity in codoped TiO_2 considering the radiation penetration depth or optical thickness in a slurry containing about 0.1 g of the material. Therefore, much of the photocatalytic enhancement can only be attributed to the absorption and activation of the material by the low energy visible light photon flux [35, 36]. Optical filters are often used to cut off any UV radiation in studies on purely visible light enhanced photocatalysis. However, in this study, simulated solar conditions were intended to mimic the natural solar conditions on a bright sunny day.

Tauc plots were used to estimate the band gaps of the materials by plotting the Tauc function versus the energy (Figure 4(c)). The absorption coefficient is related to the band energy E_g by the following equation:

$$(\alpha h\nu) = A_0\left(h\nu - E_g\right)^n, \tag{3}$$

where $h\nu$ is the photon energy, E_g is the band gap, A_0 is a parameter associated with the transition probability, and n can take the values 1/2, 2, 3/2, and 3 for direct allowed, indirect allowed, direct forbidden, and indirect forbidden transitions, respectively [37, 38]. Assuming a direct allowed transition for all the samples, band gap energies were estimated at the point of contact of the $[(\alpha h\nu) * h\nu]^2$ line to the energy axis and values tabulated (Table 2). N doping and N, metal codoping had an effect on the optical band gaps of the materials. N, PGM codoping had a profound effect on the band gaps, with N, Os TiO_2 giving the lowest (2.0 eV) followed by N, Pd TiO_2 (2.1 eV). N, base metal codoping, on the other hand, also led to band gap reductions at 2.6 eV and 2.8 eV for N, Fe TiO_2 and N, Cu TiO_2, respectively. These values are lower than those observed for the commercial P25 (3.1 eV). Thus, codoping led to shifts in the band gap energy towards longer wavelengths due to the creation of trap levels between the conduction and valence bands of TiO_2. While PGMs are much more expensive compared to base metals, they are more effective in shifting the absorption edges to the visible region in codoped TiO_2 systems [34]. This can be attributed to the type of d orbitals participating in electron transitions (3d for Fe and Cu, 4d for Pd, and 5d for Os). Devi and Kumar reported a direct relationship between band gap reduction and inverse metal dopant electronegativity. PGMs are electronegative compared to base metals, leading to higher band gap reductions [31]. Band gap reduction or red shifts in absorption edges is envisaged to improve the visible light harvesting capability of the material. This is vital in designing photocatalytic systems where abundant solar radiation may be used to activate the material as opposed to the more expensive UV sources.

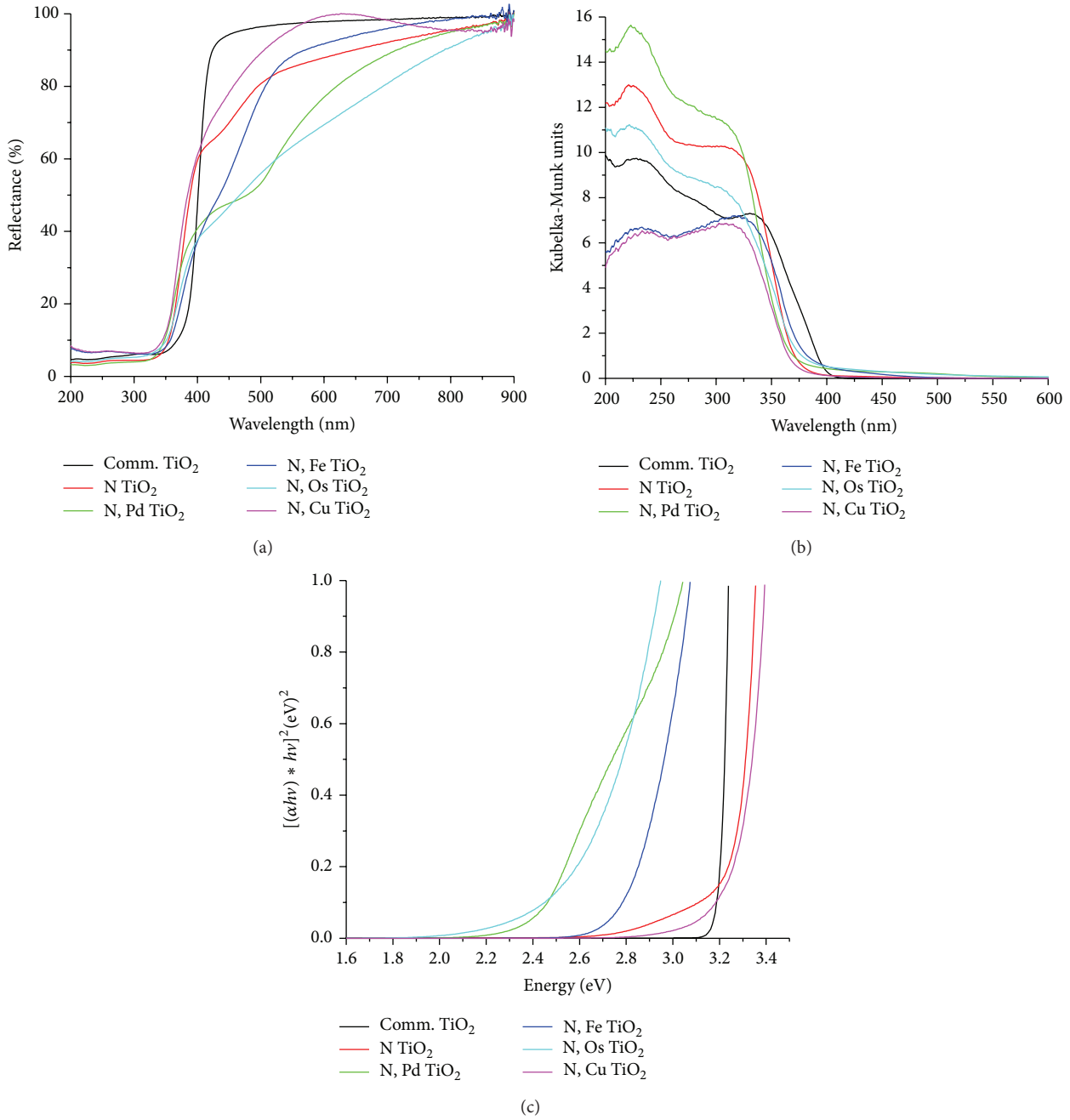

Figure 4: (a) DRUV-Vis spectra, (b) Kubelka-Munk plots, and (c) Tauc plots of the different materials.

The surface morphologies of the samples were examined by SEM (Figure 5). The samples consisted of spherical aggregates of small particles with rough surfaces. Clusters or agglomerates of the synthesised catalysts were of sizes in the range 5–10 μm. Rough estimates from the images showed that the average individual size of particles was in the nanorange.

TEM analysis was performed to probe the particle sizes and morphology of the materials (Figure 6). The N, Pd codoped TiO_2 revealed nearly spherical particles with particle size range of 20–30 nm, in agreement with XRD results (Figure 6(a)). Pd deposits, as PdO, appeared as well-dispersed small dots of about 1-2 nm on the TiO_2 particles. Therefore, it can be concluded that Pd occupies interstitial positions on the TiO_2 lattice. No particles were observed on the surface of the other codoped TiO_2 samples, an indication that the metals most likely occupy substitutional positions on the TiO_2 lattice. N, Fe TiO_2 consisted of nanoparticles with elongated and irregular spherical shapes of approximately 20 nm (Figure 6(b)). Elongated particles, some with straight edges and rectangular prism morphologies, were observed for N, Os TiO_2 and N, Cu TiO_2 and sizes were in the range 15–30 nm (Figures 6(b) and 6(c)). These observations indicate

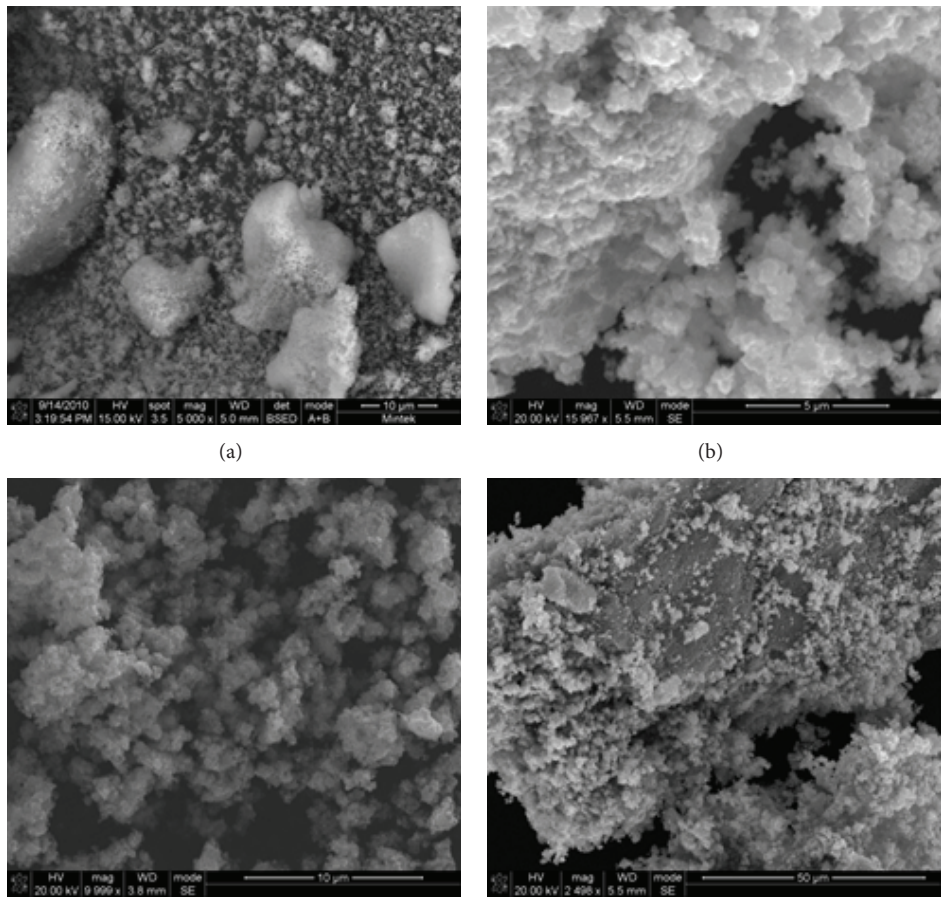

Figure 5: SEM images of (a) N, Pd TiO_2, (b) N, Fe TiO_2, (c) N, Os TiO_2, and (d) N, Cu TiO_2.

that different metal dopants have different effects on the overall size and shape of crystallites of the resulting calcined samples in N, metal codoped TiO_2.

The photoactivity of the materials was evaluated by rate of disappearance of the dye UV-Vis chromophore responsible for the peak at 515 nm. Dye suspensions were subjected to 5 minutes of sonication and an hour of continuous stirring to allow for adsorption-desorption equilibrium before illumination. There were variations in the dye adsorption capacity of the materials (Figure 7). There was some correlation between the adsorption capabilities of the materials and the photocatalytic efficiency. The highest adsorption capacity (17.5%) was noted for N, Pd TiO_2 which also showed the highest photoactivity while the lowest capacity (2.5%) for N, Cu TiO_2 correlated well with its low activity. Adsorption of molecules on the surface of the material is determined by the surface properties of the material such as surface area porosity and available surface functionalities. Presence of surface OH groups on all the materials was confirmed by FTIR studies. The OH groups are favourable adsorption sites for the dye molecules containing electronegative groups or bulky functionalities. Photocatalysis is a surface technique so the target pollutant must first be adsorbed on the surface of the material before attack by the free radicals [39]. Therefore, the greater the number of OH surface functional groups, the greater the adsorption capability and, consequently, the better the photocatalytic activity.

The photocatalytic activity of the materials was investigated by monitoring the decrease in concentration of EY at various time intervals under simulated solar light illumination (Figure 8(a)). The N, PGM codoped TiO_2 showed higher photocatalytic efficiency than the N, base metal codoped TiO_2. These observations generally correlated closely with the corresponding calculated band gap values. Nitrogen doping resulted in band gap narrowing (2.7 eV) and improved photocatalytic performance of TiO_2 under visible light irradiation compared to P25 (Table 3). Similar observations were made by a number of research groups using different synthesis methods and model pollutants [12, 40, 41]. Interestingly, the photocatalytic activity of N, Pd codoped TiO_2 was greatly enhanced with near total dye degradation (99.9%) being realised in about 90 mins. This outstanding visible light induced photocatalytic activity can be attributed to the synergistic effect of N and Pd codoping [30]. While nitrogen is an effective dopant for band reduction, PGMs, like Pd and Os used as codopants, lead to further band gap reduction and enhanced activity. Modifying the surface of TiO_2 with these electron-accepting metals that can form a Schottky barrier at

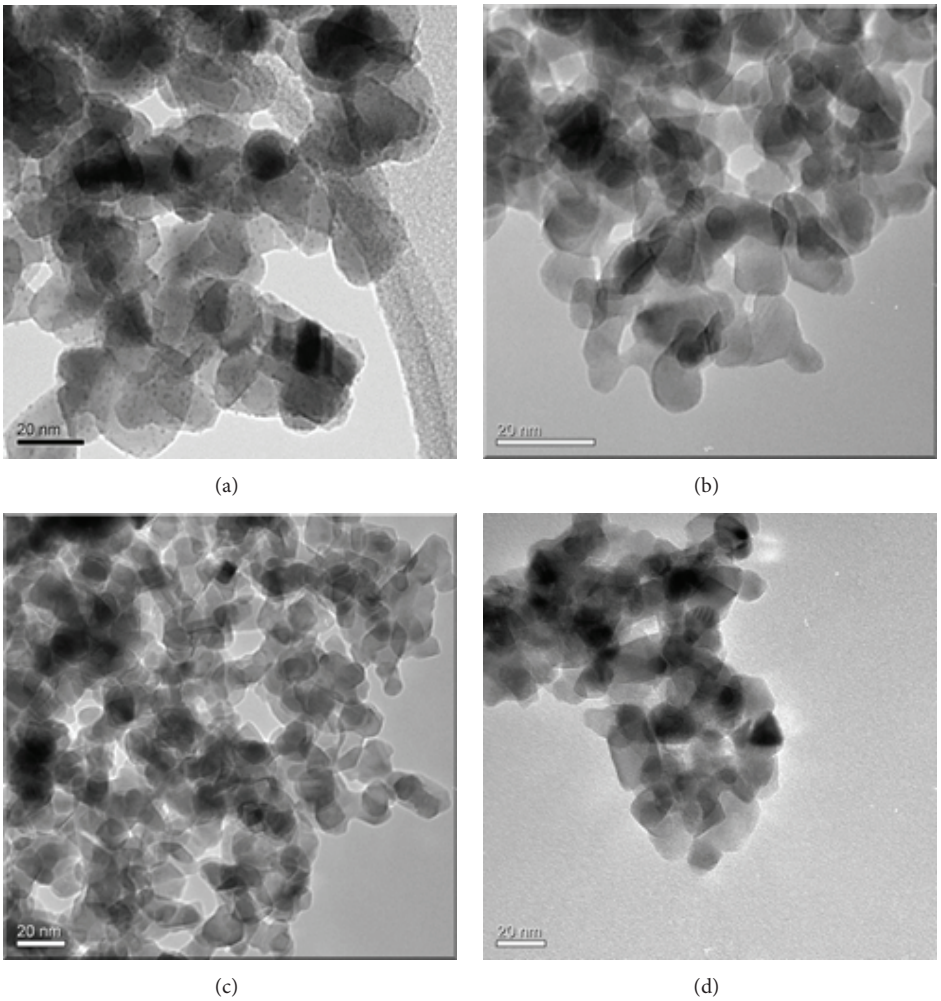

Figure 6: TEM images of (a) N, Pd TiO_2, (b) N, Fe TiO_2, (c) N, Os TiO_2, and (d) N, Cu TiO_2.

Table 3: Percentage dye degradation by the different materials.

Sample	EY degradation (%)
Comm. TiO_2 (P25)	52.6
N TiO_2	96.3
N, Pd TiO_2	99.9
N, Fe TiO_2	68.1
N, Os TiO_2	91.7
N, Cu TiO_2	25.5

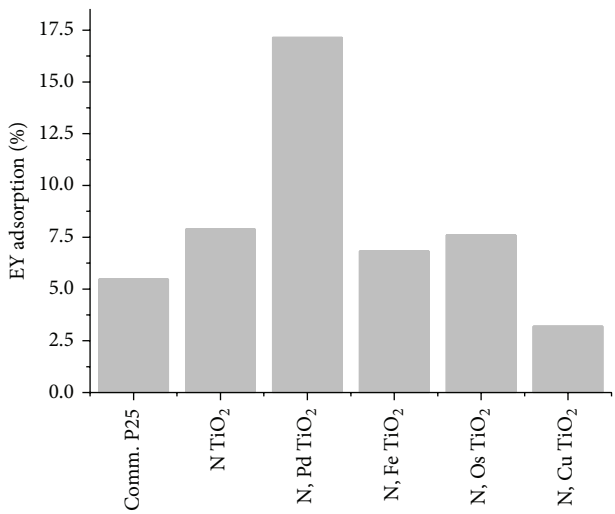

Figure 7: Percentage dye adsorption on different materials.

the metal/TiO_2 interface means that they can act as electron sinks and thus retard electron-hole recombination [38, 42].

Base metals have also been used as dopants individually or on as codopants on TiO_2. Recently, base metals (Cr, Mn, Fe, Co, Ni, Cu, and Zn) were used to replace noble metals as TiO_2 dopants to reduce the overall catalyst production costs. Fe-doped TiO_2 was reported to show high dye-degradation efficiency of 90% and 75% total organic carbon (TOC) removal efficiency of Acid Blue 92 upon UV light irradiation. The incorporation of base metal ions onto the TiO_2 lattice was found to alter or lower the band gap energy and shift the catalyst absorbance edge closer to the visible region [8]. A similar trend was observed for the N, Fe codoped TiO_2

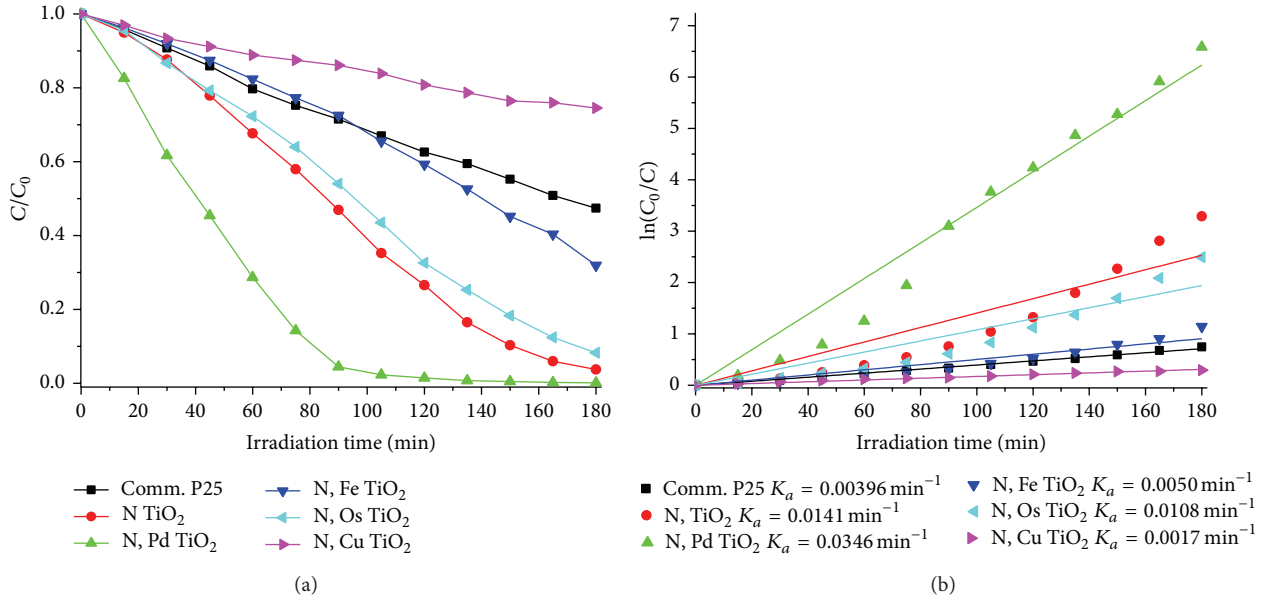

FIGURE 8: (a) Photodegradation profile and (b) photodegradation kinetics of the different samples.

where there was appreciable band gap reduction associated with some catalytic enhancement. N, Cu TiO_2 on the other hand showed the lowest photoactivity under the same experimental conditions. This can be attributed to the lower band gap reduction effect (2.8 eV) as well as the possibility of the dopants acting as electron-hole recombination centres.

The Langmuir-Hinshelwood (LH) kinetics is the most commonly used model for heterogeneous catalytic processes for the photodegradation of organic contaminants in solution. Application of this model to an ideal batch reactor produces a simplified expression [38, 43]:

$$-\ln\left(\frac{C}{C_0}\right) = k_{\text{app}}t, \tag{4}$$

where C is the concentration of the molecule being degraded, C_0 is the initial concentration of organic molecules being degraded, k_{app} is the apparent rate constant, and t is the irradiation time. A plot of $\ln(C_0/C)$ versus t will yield a graph with a slope of k_{app} (Figure 8(b)).

Linearity of the plots suggests that the photodegradation reaction approximately follows first order kinetics with k_{app} values from 0.0017 min^{-1} to 0.0346 min^{-1}. The introduction of nitrogen and palladium onto the TiO_2 matrix drastically increased the rate constant to 0.0346 min^{-1} compared to commercial P25 TiO_2 (0.00396 min^{-1}). In comparison, the other N, PGM codoped sample (N, Os codoped TiO_2) showed a lower rate constant (0.0108 min^{-1}) which was almost similar to that of N doped TiO_2 (0.0141 min^{-1}). Codoping with base metals led to a slight improvement in photoactivity for N, Fe TiO_2 (0.0050 min^{-1}) and poor photoactivity and lower photodegradation rate for N, Cu TiO_2 (0.0017 min^{-1}) compared to commercial P25. The lower rates can be attributed to the poor electron trapping capability of the base metals compared to PGMs. Low band gap red shifts led to poor visible light harvesting capacity for the N, base metal codoped TiO_2 samples. There are many variables in the photocatalytic chain of events that can result in lower degradation rates; photons may not be absorbed but scattered out of the reactor; photons may be absorbed but fail to create an electron/hole pair, especially if the energy of the photon is close to the energy of band gap; electron/hole pairs may not make it to the surface of the particle but instead recombine inside the particle. PdO is reported as a p-type semiconductor with band gap values from 0.1 to 2.7 eV. Both the conduction band and the valence band of PdO nanoparticles lie between those of TiO_2; thus the photogenerated electrons from TiO_2 conduction band can easily be channeled to the PdO conduction band while the holes from the TiO_2 valence band can also be partially trapped in the PdO valence band before scavenging water molecules to generate highly reactive OH radicals. Therefore, the photo induced electron transfer that occurs from TiO_2 to PdO nanoparticles prolongs the lifetime of electron-hole pairs. It is also widely accepted that PdO is a more effective electron acceptor than Pd, which further contributes to its effectiveness in enhanced photocatalytic activity. Finally, even when electrons and holes become trapped at the surface, they may fail to induce the surface reaction. These factors, together with the normal mass transfer limitations and losses due to imperfect mixing and uncertainties in photon fluxes, have an effect on the observed photodegradation rates [44].

Irradiation of TiO_2 with UV light generates conduction band electrons (e^-) and valence band holes (h^+) (Figure 9). The holes can scavenge surface hydroxyl ions or water to produce hydroxyl radicals ($OH^\bullet$), while electrons can react with adsorbed molecular oxygen yielding superoxide anion radicals ($O_2^\bullet$). The superoxide anion radicals can act as oxidising agents or as additional sources of hydroxyl radicals when they react with water molecules. Theoretically, the pure

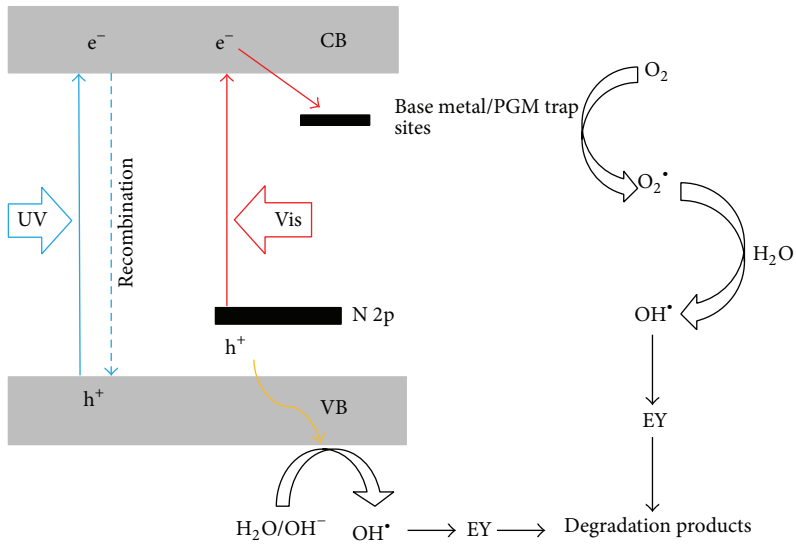

FIGURE 9: Schematic illustration of the proposed spatial distribution of electrons/holes and the generation of free radicals for EY degradation in a codoped TiO_2 system.

TiO_2 cannot be excited by visible light because of its high band gap energy (3.2 eV). Introduction of nitrogen creates energy states closer to the valence band within the TiO_2 band gap. This reduces the band gap of the N doped TiO_2, extending the absorption edge well into the visible region. The excited electrons can quickly recombine with the holes, losing energy in the form of heat. However, in the presence of metals, which also form energy states within the TiO_2 band gap, a Schottky barrier is formed at the semiconductor-metal interface causing some band bending. This electron deficiency region acts as an electron sink, trapping the electrons and prolonging the lifetime of holes. The overall effect is retardation of charge carrier recombination rate coupled with preferential formation of the highly oxidative hydroxyl radicals that can mineralise organic compounds such as dyes to harmless products, water, and carbon dioxide [34].

4. Conclusion

Nitrogen, base metal and nitrogen, PGM codoped TiO_2 nanoparticles were successfully synthesised by a simple modified sol-gel technique and evaluated for their visible light photocatalytic activities. The materials consisted mainly of the anatase phase after calcination at 500°C. Codoping led to a red shift in the absorption edge of the materials and this was confirmed by the reduction in the band gaps. TEM analysis verified the presence of uniformly dispersed and very small (5 nm) PdO particles deposited on the TiO_2 in N, Pd TiO_2. The metals in the other samples were most likely incorporated into the lattice of TiO_2 as there was no visible evidence of their presence from TEM analysis. The N, PMG codoped TiO_2 showed significantly enhanced photocatalytic activity compared to the N, base metal codoped samples under visible light irradiation. These results indicate that formation of a Schottky barrier at the metal-TiO_2 interface creates electron trap sites that act as electron sinks, prolonging the lifetime of holes for enhanced photoactivity. This effect was more pronounced for PGMs compared to base metals. While the use of PGMs (Pd and Os) as TiO_2 dopants in wastewater treatment may prove uneconomical because of their high cost and scarcity, their catalytic effect proved to be better than that of the cheaper and readily available base metals in N, metal codoped TiO_2. Therefore, a compromise may need to be considered between cost, availability, and efficiency in selecting the best TiO_2 metal dopants for water decontamination.

Conflict of Interests

The authors declare that there is no conflict of interests regarding the publication of this paper.

Acknowledgments

Funding from DST/Mintek Nanotechnology Innovation Centre is appreciated.

References

[1] M. R. Hoffmann, S. T. Martin, W. Choi, and D. W. Bahnemann, "Environmental applications of semiconductor photocatalysis," *Chemical Reviews*, vol. 95, no. 1, pp. 69–96, 1995.

[2] A. V. Rupa, D. Divakar, and T. Sivakumar, "Titania and noble metals deposited titania catalysts in the photodegradation of tartazine," *Catalysis Letters*, vol. 132, no. 1-2, pp. 259–267, 2009.

[3] P. Wu, R. Xie, and J. K. Shang, "Enhanced visible-light photocatalytic disinfection of bacterial spores by palladium-modified nitrogen-doped titanium oxide," *Journal of the American Ceramic Society*, vol. 91, no. 9, pp. 2957–2962, 2008.

[4] M. Anpo and M. Takeuchi, "The design and development of highly reactive titanium oxide photocatalysts operating under

visible light irradiation," *Journal of Catalysis*, vol. 216, no. 1-2, pp. 505–516, 2003.

[5] A. Kafizas, S. Kellici, J. A. Darr, and I. P. Parkin, "Titanium dioxide and composite metal/metal oxide titania thin films on glass: a comparative study of photocatalytic activity," *Journal of Photochemistry and Photobiology A: Chemistry*, vol. 204, no. 2-3, pp. 183–190, 2009.

[6] S. Sato, "Photocatalytic activity of NO_x-doped TiO_2 in the visible light region," *Chemical Physics Letters*, vol. 123, no. 1-2, pp. 126–128, 1986.

[7] D. Dvoranova, V. Brezova, M. Mazur, and M. A. Malati, "Investigations of metal-doped titanium dioxide photocatalysts," *Applied Catalysis B: Environmental*, vol. 37, no. 2, pp. 91–105, 2002.

[8] S. H. S. Chan, T. Y. Wu, J. C. Juan, and C. Y. The, "Recent developments of metal oxide semiconductors as photocatalysts in advanced oxidation processes (AOPs) for treatment of dye waste-water," *Journal of Chemical Technology and Biotechnology*, vol. 86, no. 9, pp. 1130–1158, 2011.

[9] M. Zhou, J. Yu, and B. Cheng, "Effects of Fe-doping on the photocatalytic activity of mesoporous TiO_2 powders prepared by an ultrasonic method," *Journal of Hazardous Materials*, vol. 137, no. 3, pp. 1838–1847, 2006.

[10] Y. Cong, F. Chen, J. Zhang, and M. Anpo, "Carbon and nitrogen-codoped TiO_2 with high visible light photocatalytic activity," *Chemistry Letters*, vol. 35, no. 7, pp. 800–801, 2006.

[11] H. Liu and L. Gao, "(Sulfur, nitrogen)-codoped rutile-titanium dioxide as a visible-light-activated photocatalyst," *Journal of the American Ceramic Society*, vol. 87, no. 8, pp. 1582–1584, 2004.

[12] R. Asahi, T. Morikawa, T. Ohwaki, K. Aoki, and Y. Taga, "Visible-light photocatalysis in nitrogen-doped titanium oxides," *Science*, vol. 293, no. 5528, pp. 269–271, 2001.

[13] Y. Suda, H. Kawasaki, T. Ueda, and T. Ohshima, "Preparation of high quality nitrogen doped TiO_2 thin film as a photocatalyst using a pulsed laser deposition method," *Thin Solid Films*, vol. 453-454, pp. 162–166, 2004.

[14] K. S. Rane, R. Mhalsiker, S. Yin et al., "Visible light-sensitive yellow $TiO_{2-x}N_x$ and Fe-N co-doped $Ti_{1-y}Fe_yO_{2-x}N_x$ anatase photocatalysts," *Journal of Solid State Chemistry*, vol. 179, no. 10, pp. 3033–3044, 2006.

[15] T. Tachikawa, S. Tojo, K. Kawai et al., "Photocatalytic oxidation reactivity of holes in the sulfur- and carbon-doped TiO_2 powders studied by time-resolved diffuse reflectance spectroscopy," *Journal of Physical Chemistry B*, vol. 108, no. 50, pp. 19299–19306, 2004.

[16] Q. Li, R. Xie, W. L. Yin, E. A. Mintz, and K. S. Jian, "Enhanced visible-light-induced photocatalytic disinfection of *E. coli* by carbon-sensitized nitrogen-doped titanium oxide," *Environmental Science and Technology*, vol. 41, no. 14, pp. 5050–5056, 2007.

[17] Y. Sakatani, H. Ando, K. Okusako et al., "Metal ion and N co-doped TiO_2 as a visible-light photocatalyst," *Journal of Materials Research*, vol. 19, no. 7, pp. 2100–2108, 2004.

[18] Y. Sakatani, J. Nunoshige, H. Ando et al., "Photocatalytic Decomposition of Acetaldehyde under Visible Light Irradiation over La^{3+} and N Co-doped TiO_2," *Chemistry Letters*, vol. 32, no. 12, pp. 1156–1157, 2003.

[19] D. Li, H. Haneda, S. Hishita, and N. Ohashi, "Visible-light-driven N-F-codoped TiO_2 photocatalysts. 1. Synthesis by spray pyrolysis and surface characterization," *Chemistry of Materials*, vol. 17, no. 10, pp. 2588–2595, 2005.

[20] Y. Li, G. Ma, S. Peng, G. Lu, and S. Li, "Boron and nitrogen co-doped titania with enhanced visible-light photocatalytic activity for hydrogen evolution," *Applied Surface Science*, vol. 254, no. 21, pp. 6831–6836, 2008.

[21] M. Xing, Y. Wu, J. Zhang, and F. Chen, "Effect of synergy on the visible light activity of B, N and Fe co-doped TiO_2 for the degradation of MO," *Nanoscale*, vol. 2, no. 7, pp. 1233–1239, 2010.

[22] Q. Li, R. Xie, E. A. Mintz, and J. K. Shang, "Enhanced visible-light photocatalytic degradation of humic acid by palladium-modified nitrogen-doped titanium oxide," *Journal of the American Ceramic Society*, vol. 90, no. 12, pp. 3863–3868, 2007.

[23] D. Li, Z. Chen, Y. Chen et al., "A new route for degradation of volatile organic compounds under visible light: using the bifunctional photocatalyst $Pt/TiO_{2-x}N_x$ in H_2-O_2 atmosphere," *Environmental Science & Technology*, vol. 42, no. 6, pp. 2130–2135, 2008.

[24] M. A. Henderson, "A surface science perspective on TiO_2 photocatalysis," *Surface Science Reports*, vol. 66, no. 6-7, pp. 185–297, 2011.

[25] C. Wen, Y.-J. Zhu, T. Kanbara, H.-Z. Zhu, and C.-F. Xiao, "Effects of I and F codoped TiO_2 on the photocatalytic degradation of methylene blue," *Desalination*, vol. 249, no. 2, pp. 621–625, 2009.

[26] T.-H. Kima, V. Rodríguez-González, G. Gyawalia, S.-H. Choa, T. Sekinoc, and S.-W. Lee, "Synthesis of solar light responsive Fe, N co-doped TiO_2 photocatalyst by sonochemical method," *Catalysis Today*, vol. 212, pp. 75–80, 2013.

[27] Y. Cong, J. Zhang, F. Chen, M. Anpo, and D. He, "Preparation, photocatalytic activity, and mechanism of nano-TiO_2 Co-doped with nitrogen and iron (III)," *Journal of Physical Chemistry C*, vol. 111, no. 28, pp. 10618–10623, 2007.

[28] F. M. Dukes, E. Iuppa, B. Meyer, and M. J. Shultz, "Differing photo-oxidation mechanisms: electron transfer in TiO_2 versus iron-doped TiO_2," *Langmuir*, vol. 28, no. 49, pp. 16933–16940, 2012.

[29] A. T. Kuvarega, R. W. M. Krause, and B. B. Mamba, "Photocatalytic performance of nitrogen, osmium co-doped TiO_2 for removal of eosin yellow in water under simulated solar radiation," *Journal of Nanoscience and Nanotechnology*, vol. 13, no. 7, pp. 5017–5027, 2013.

[30] H. Liu, Y. Wu, and J. Zhang, "A new approach toward carbon-modified vanadium-doped titanium dioxide photocatalysts," *ACS Applied Materials and Interfaces*, vol. 3, no. 5, pp. 1757–1764, 2011.

[31] L. G. Devi and S. G. Kumar, "Influence of physicochemical-electronic properties of transition metal ion doped polycrystalline titania on the photocatalytic degradation of Indigo Carmine and 4-nitrophenol under UV/solar light," *Applied Surface Science*, vol. 257, no. 7, pp. 2779–2790, 2011.

[32] S. S. Thind, G. Wu, and A. Chen, "Synthesis of mesoporous nitrogen-tungsten co-doped TiO_2 photocatalysts with high visible light activity," *Applied Catalysis B: Environmental*, vol. 111-112, pp. 38–45, 2012.

[33] A. T. Kuvarega, R. W. M. Krause, and B. B. Mamba, "Nitrogen/palladium-codoped TiO_2 for efficient visible light photocatalytic dye degradation," *Journal of Physical Chemistry C*, vol. 115, no. 45, pp. 22110–22120, 2011.

[34] K. Yamanaka, T. Ohwaki, and T. Morikawa, "Charge-carrier dynamics in Cu- or Fe-loaded nitrogen-doped TiO_2 powder studied by femtosecond diffuse reflectance spectroscopy," *The Journal of Physical Chemistry C*, vol. 117, no. 32, pp. 16448–16456, 2013.

[35] M. A. Mueses, F. Machuca-Martinez, and G. Li Puma, "Effective quantum yield and reaction rate model for evaluation of photocatalytic degradation of water contaminants in heterogeneous pilot-scale solar photoreactors," *Chemical Engineering Journal*, vol. 215-216, pp. 937–947, 2013.

[36] D. Friedmann, C. Mendive, and D. Bahnemman, "TiO_2 for water treatment: parameters affecting the kinetics and mechanisms of photocatalysis," *Applied Catalysis B: Environmental*, vol. 99, no. 3-4, pp. 398–406, 2010.

[37] W. E. Mahmoud, A. A. Al-Ghamdi, and F. Al-Agel, "Synthesis and optical properties of poly (vinyl acetate)/bismuth oxide nanorods," *Polymers for Advanced Technologies*, vol. 22, no. 12, pp. 2055–2061, 2011.

[38] B. Ohtani, "Photocatalysis A to Z-What we know and what we do not know in a scientific sense," *Journal of Photochemistry and Photobiology C: Photochemistry Reviews*, vol. 11, no. 4, pp. 157–178, 2010.

[39] M. N. Chong, B. Jin, C. W. K. Chow, and C. Saint, "Recent developments in photocatalytic water treatment technology: a review," *Water Research*, vol. 44, no. 10, pp. 2997–3027, 2010.

[40] T. Morikawa, R. Asahi, T. Ohwaki, K. Aoki, and Y. Taga, "Band-gap narrowing of titanium dioxide by nitrogen doping," *Japanese Journal of Applied Physics, Part 2: Letters*, vol. 40, no. 6A, pp. L561–L563, 2001.

[41] H. Irie, Y. Watanabe, and K. Hashimoto, "Nitrogen-concentration dependence on photocatalytic activity of $TiO_{2-x}N_x$powders," *Journal of Physical Chemistry B*, vol. 107, no. 23, pp. 5483–5486, 2003.

[42] E. Kowalska, O. O. P. Mahaney, R. Abe, and B. Ohtani, "Visible-light-induced photocatalysis through surface plasmon excitation of gold on titania surfaces," *Physical Chemistry Chemical Physics*, vol. 12, no. 10, pp. 2344–2355, 2010.

[43] N. G. Asenjo, R. Santamaría, C. Blanco, M. Granda, P. Álvarez, and R. Menéndez, "Correct use of the Langmuir-Hinshelwood equation for proving the absence of a synergy effect in the photocatalytic degradation of phenol on a suspended mixture of titania and activated carbon," *Carbon*, vol. 55, pp. 62–69, 2013.

[44] M. Motegh, J. Cen, P. W. Appel, J. R. van Ommen, and M. T. Kreutzer, "Photocatalytic-reactor efficiencies and simplified expressions to assess their relevance in kinetic experiments," *Chemical Engineering Journal*, vol. 207-208, pp. 607–615, 2012.